JOURNAL OF CATALYSIS 117, 467–484 (1989)

The Mechanism and Kinetics of Methane Formation by Decomposition of Methanol on a Ni/SiO_2 Catalyst

P. K. DE BOKX, A. R. BALKENENDE, AND J. W. GEUS

Department of Inorganic Chemistry, University of Utrecht, Croesestraat 77A, 3522 AD Utrecht, The Netherlands

Received August 10, 1987; revised November 21, 1988

The rate of methane formation by decomposition of methanol is studied at temperatures between 473 and 583 K and methanol pressures between 0.2 and 10.4 kPa. Coverages of adsorbed species are measured using temperature-programmed hydrogenation (TPH), temperature-programmed desorption (TPD), and magnetic measurements. The reaction system can be adequately described assuming the decomposition of methanol to proceed in two steps, viz. a decomposition into CO and H_2 followed by methanation of CO. The former reaction is much more rapid than the latter. Assuming CH hydrogenation to be rate-determining, the rate of methane formation could be described by the LHHW rate equation

$$\mathrm{TOF} = \frac{1.2 \times 10^5 e^{-68/RT} p^{1.5}}{(1 + 1.8 \times 10^{-1} e^{15/RT} p^{0.5} + 3.1 \times 10^{-16} e^{144/RT} p)^2}.$$

TOF is the turnover frequency in s^{-1}, p is the methanol pressure in kPa, T is the temperature in K, and $R = 8.314 \times 10^{-3}$ kJ mol^{-1} K^{-1}. Coverages of adsorbed species predicted by this equation differ strongly from results obtained by measurements of total surface coverages using TPH, TPD, and magnetic measurements. This has been interpreted as an indication that the number of surface sites actively participating in the methanation reaction composes only a small fraction of the total number of sites.

INTRODUCTION

The decomposition of methanol over nickel and other Group VIII metals has been the subject of a great number of investigations (*1–11*). The majority of these studies pertain to conditions where both thermodynamics (UHV conditions) and kinetics (short contact times) favor decomposition into carbon monoxide and hydrogen, according to

$$CH_3OH \rightleftharpoons CO + 2H_2. \qquad (1)$$

This decomposition probably proceeds via successive dehydrogenation steps in which methanol is converted to CO and H_2 via methoxy intermediates. The dehydrogenation of CH_3O(ad) is thought to be the rate-determining step (*6, 7*).

Relatively little research effort has been devoted to the study of reactions occurring under conditions where methane is formed as a product of the methanol decomposition (*8–11*). Production of methane via methanol decomposition has received some attention recently due to the possible use of methanol as a transportation fuel. Provided the transportation distance is sufficiently large, the conversion of natural gas to methane followed by transportation and regasification of the methanol appears to be more attractive than transportation of liquefied natural gas (*12, 13*).

Several mechanisms have been proposed to explain methane formation from methanol. Some authors claim that methane is formed form methanol either via abstraction of the oxygen atom (*8*) or via abstraction of the hydroxyl group followed by hydrogenation of the remaining methyl group (*9*). It has also been suggested that methane is formed in a two-step process: methanol initially decomposes into CO and H_2 fol-

0021-9517/89 $3.00

lowed by the methanation of carbon monoxide (*10, 11*).

This latter reaction has been studied extensively in recent years and excellent reviews have been published (*14–16*). It is generally accepted that methane is formed via hydrogenation of an adsorbed carbonaceous species. There is some argument concerning the detailed mechanism. Although there have been several reports in which hydrogen-assisted CO dissociation was proposed, the majority of recent investigations seem to be in favor of a mechanism in which CO is dissociated, followed by hydrogenation of adsorbed oxygen and carbon. The position of the rate-determining step has not been unequivocally established.

The advancement of the decomposition of methanol into CO and H_2 can be described by a single parameter, viz. the extent of reaction. We are thus dealing with a single stoichiometric reaction (*17*). Under the conditions where methane is formed, this is no longer the case. A number of single stoichiometric reactions are required to described the advancement of the methanol decomposition. Such a reaction system is generally denoted as complex; i.e., the advancement of the reaction can no longer be described by a single parameter, at least two parameters being needed. This investigation has been undertaken (i) to identify the (dominant) reactions leading to methane, (ii) to obtain information on the sequence of elementary steps, and (iii) to determine the position of the rate-determining step in this sequence.

The reaction system has been analyzed using the combinatorial technique developed by Happel and Sellers (*18*). Rate equations are derived by putting the rate-determining step at different positions in the sequence of elementary steps of the derived mechanism. The derived rate equations are tested using kinetic data obtained from stationary-state measurements at temperatures between 473 and 583 K and methanol pressures ranging from 0.2 to 10.4 kPa. Kinetic data are supplemented by measurements of surface coverages using temperature-programmed hydrogenation (TPH), temperature-programmed desorption (TPD), and magnetic measurements.

EXPERIMENTAL

Materials

The 50 wt% Ni/SiO_2 catalyst used in this study was prepared by precipitation of Ni^{2+} ions onto suspended silica (Degussa 380V) by means of urea decomposition at 363 K (*19*). The catalyst was dried overnight at 393 K, pressed (150 MPa), and cut into pellets (0.15–0.30 mm). Dehydration and reduction were carried out in the reactor in a 10% H_2/N_2 flow (58 ks at 393 K, 260 ks at 723 K, according to (*20*)). Relevant physical properties of the catalyst are collected in Table 1.

TABLE 1

Physical Properties of the Catalyst

Property	Value	Technique
Degree of reduction	70 ± 5%	High-field magnetization measurements (77 K)
Dispersion	14 ± 2%	H_2 chemisorption (298 K)
	20 ± 2%	Magnetization measurements (298 K)
Ni surface area	90 ± 9 m^2/g metal. Ni	H_2 chemisorption (298 K)
	34 ± 3 m^2/g red. cat.	
Particle diameter	7.0 ± 0.7 nm	H_2 chemisorption (298 K)
Pore volume	0.43 ± 0.02 ml/g	N_2 physisorption (77 K)
BET surface area	256 ± 2 m^2/g	N_2 physisorption (77 K)

All gases were supplied by Hoek-Loos Co. Hydrogen and nitrogen were successively passed through columns containing a Deoxo catalyst (BASF R 3-11) and a molecular sieve (Linde 4A) to remove traces of oxygen and water, respectively. Carbon monoxide was used without purification. Methanol (Baker p.a.) could be introduced into the gas stream in accurately known amounts using an apparatus described by Davydov and Kharson (*21*).

Apparatus

Kinetic measurements were performed using a continuous flow system (*22*). A quartz microreactor (i.d. 10 mm) was employed in all experiments. In a gas-mixing system two separate gas flows consisting of (a mixture of) N_2, H_2, CO, or CH_3OH could be prepared. The flow rates were accurately regulated by mass flow controllers (PFD-914). The flow fed to the reactor could be instantaneously replaced by the second flow by means of two four-way valves. This procedure was applied when quenching from a stationary-state was carried out.

The analyzing system consisted of a Perkin–Elmer Sigma IB gas chromatographic system equipped with a 3.0-m stainless-steel column packed with Porapak QS. Separation of gas mixtures was carried out using the following temperature program: 180 s isothermal operation at 333 K, a temperature ramp of 0.16 K/s to 413 K, followed by 420 s isothermal operation at this temperature. This temperature program was found to yield a good compromise between fast elution of CH_3OH and complete separation of CO and CH_4. Samples were drawn from the gas stream by means of pneumatic sampling valves (Valco). Quantitative analyses were obtained using a hot-wire detector (HWD) and a flame ionization detector (FID) in series. Between HWD and FID a catalytic reactor (Perkin–Elmer) was installed to convert carbon-containing compounds quantitatively to methane, thereby greatly increasing the detection sensitivity. All carbon-containing gases (CH_4, CO, CO_2, CH_3OH, C_2H_6) could thus be detected with an accuracy better than 1%. Hydrogen was measured with a low accuracy, due to the short retention time of H_2, which causes the peak to coincide partly with the N_2-pressure pulse peak needed for sampling. Small amounts of water could not be quantitatively determined.

Measurements were automated using a computer program controlling the reactor temperature, the sampling frequency, and the data acquisition. All results were transmitted to a Cyber 180-855 computer for storage and subsequent calculations.

TPH and TPD of adsorbed species were performed in the same apparatus as that used for the kinetic measurements. The employed gas chromatographic detection limited linear heating rates to 10 mK/s.

Saturation magnetizations could be measured in the same reactor as that used for the kinetic, TPH, and TPD studies. A modified Weiss extraction technique was used, applying magnetic field strengths up to 0.52 MA/m and temperatures ranging between 100 and 740 K (*23*).

Procedure

Typically 15–100 mg of the pelleted catalyst was brought into the microreactor and pretreated *in situ*. A methanol pressure and flow rate were selected. After attainment of the stationary state, usually within 1.2 ks, the effluent composition was monitored for at least 3.6 ks. Provided the conversion to methane did not exceed 8%, the average of the measurements was used for the evaluation of the turnover frequency (TOF), assuming ideal differential plug-flow behavior (*17*). Stationary-state measurements were performed at a series of temperatures. At the end of such a series the initial measurement was repeated in order to check on deactivation of the catalyst. The deactivation never exceeded 5% after 87 ks operation at various temperatures. Before this procedure was repeated at a subsequent methanol pressure and flow rate the catalyst was

reduced for 7.2 ks at 723 K to restore its original activity.

The absence of rate limitations by interphase and intraparticle heat and mass transfer was checked using the Koros/Nowak criterion (*24, 25*). Over a range of temperatures (473–583 K) it was verified that diluting the catalyst with silica in a one-to-three ratio did not influence the observed turnover frequencies. It has recently been shown by Madon and Boudart (*25*) that under conditions where the above criterion is obeyed ideal plug-flow behavior is also guaranteed.

TPH and TPD experiments were always carried out in combination with magnetic measurements. Approximately 180 mg of catalyst was brought into the reactor. TPH experiments were always conducted with a 10 vol% H_2/N_2 mixture at a flow rate of 1.0 ml/s. TPD was performed in a N_2 flow at a flow rate of 0.7 ml/s.

RESULTS

Thermodynamics

Many studies on the decomposition of methanol have been performed under conditions (low total pressure) where, according to thermodynamics, decomposition into CO and H_2 is favored. To investigate both the equilibria that could be attained under our conditions and the performance of the catalyst, measurements at high residence times have been carried out in conjunction with thermodynamic calculations.

In Fig. 1 the effluent compositions obtained at a residence time of 20 s are plotted as a function of temperature. The gas fed to the reactor consisted of 7.1 kPa methanol balanced with nitrogen. The curves in the figure correspond to equilibrium compositions that have been obtained using the method described by White *et al.* (*26*). The method essentially consists of minimizing the Gibbs free energy of a mixture of known compounds constrained by a mass balance. A modified Newton minimization procedure has been used to obtain the solutions

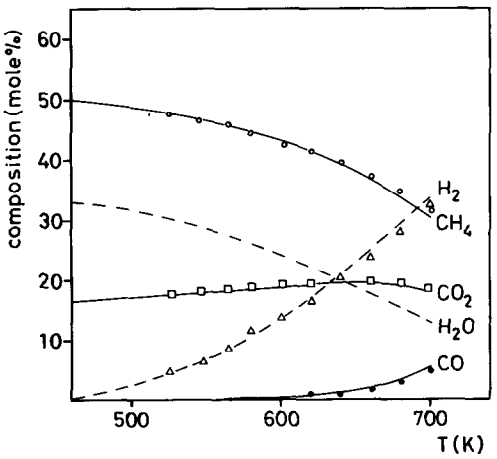

FIG. 1. Effluent gas compositions obtained at a residence time of 20 s and a methanol pressure of 7.1 kPa. The curves correspond to calculated equilibrium compositions.

(*27*). It was assumed that reactions leading to solid carbon did not proceed. As can be seen from Fig. 1 experimental equilibrium compositions are indeed not measurably influenced by reactions to solid carbon. The equilibrium composition strongly depends on the temperature. At low temperatures the overall reaction can be described by

$$4CH_3OH \rightleftharpoons 3CH_4 + CO_2 + 2H_2O. \quad (2)$$

Kinetics

In Fig. 2 a typical plot of effluent gas compositions as a function of residence time is shown. Small quantities of C_2H_6 could be detected at short residence times, but never amounted to more than 0.6 mol% of the effluent gas and have not been included in the figure. At short residence times CH_3OH decomposes into CO and H_2, whereas CH_4 is formed only at longer residence times. Another significant result is the observation that carbon dioxide formation does not occur at low conversions of methanol to methane. The reaction rates for methane formation presented below have all been obtained under differential conditions, i.e., at residence times shorter than 1.5 s. This implies that initial rates

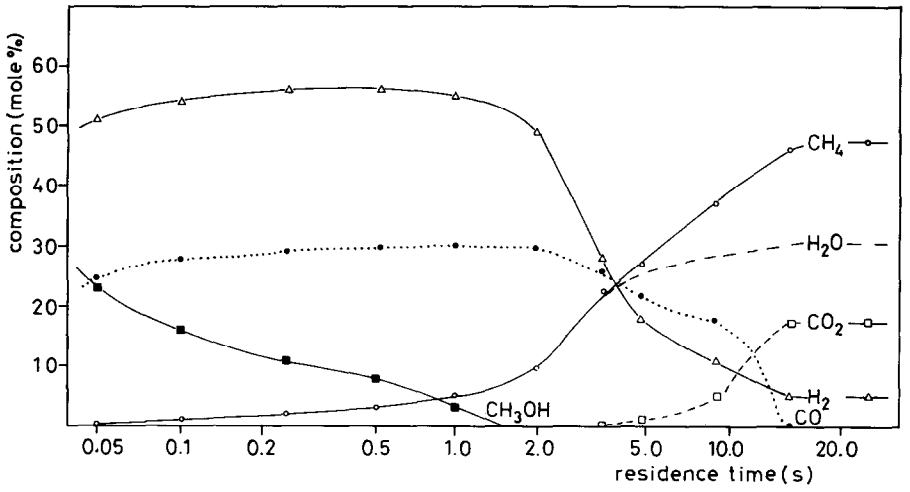

FIG. 2. Effluent gas composition as a function of residence time at a methanol pressure of 7.1 kPa and a temperature of 523 K.

were measured. It should be stressed that under these conditions no carbon dioxide was detected.

A number of 159 data sets were collected within a methanol pressure range of 0.2–10.4 kPa and a temperature range of 473–583 K. The residence times were varied between 0.04 and 1.5 s. The pure SiO_2 support did not show any activity. Rates are expressed as turnover frequencies (molecules CH_4 formed per site per second, assuming 1.54×10^{19} sites/m^2 Ni (*28*)). The observed methanation rates spanned three orders of magnitude. The reproducibility of individual data points, obtained with one catalyst batch, was better than 5%. Larger deviations, up to 10%, were observed between different catalyst batches due to differences in the pretreatment procedure.

The influence of the pressure on the rate of methane formation is illustrated in Fig. 3, where representative results measured at three temperatures are shown. Over our pressure range no marked influence of the temperature on the reaction order was observed. In Fig. 4 the temperature dependence of the reaction rate is analogously exemplified. A slight but significant decrease of the activation energy with increasing temperature is observed.

Finally, it is demonstrated in Fig. 5 that a CO/H_2 mixture of a ratio of 0.5 gives rise to methane formation rates equal to those obtained via methanol decomposition, provided the CO and CH_3OH partial pressures are equal.

Surface Coverages

To determine the coverages of surface intermediates during the stationary state, a combination of temperature-programmed hydrogenation, temperature-programmed desorption, and magnetic measurements was performed.

The catalyst was reduced *in situ* and

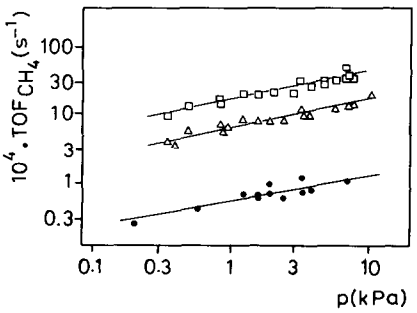

FIG. 3. Dependence of methane formation rates on methanol partial pressure at 476 K (●), 518 K (△), and 537 K (□).

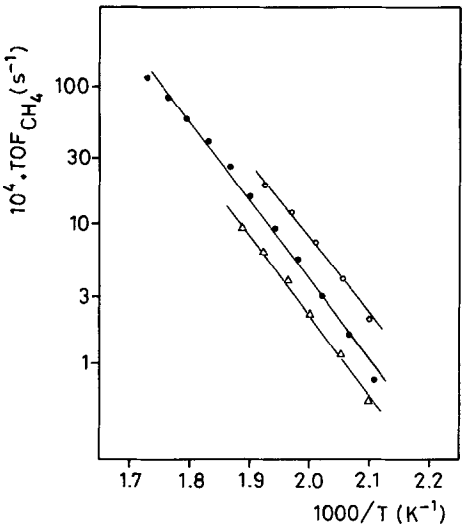

FIG. 4. Arrhenius plot of methane formation rate at methanol partial pressures of 1.0 kPa (△), 3.8 kPa (●), and 10.2 kPa (○).

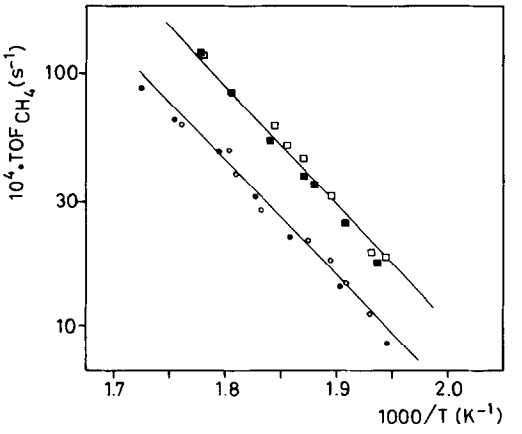

FIG. 5. Comparison of methanation rates for methanol (○, $p_{methanol}$ = 4.6 kPa; □, $p_{methanol}$ = 8.0 kPa) and CO/H_2 = 0.5 mixtures (●, p_{CO} = 4.8 kPa; ■, p_{CO} = 8.1 kPa).

slowly cooled to room temperature. The magnetization of the catalyst saturated with hydrogen was determined ((●) in Fig. 6). The sample was subsequently flushed with N_2 at 698 K for 7.2 ks and the magnetization of the clean catalysts was measured ((△) in Fig. 6). Saturation magnetizations were determined by extrapolating from magnetic field strengths between 0.35 and 0.52 MA/m to infinite fields according to the method described by Selwood (*29*). The difference in saturation magnetization between the hydrogen-saturated catalyst and the clean catalyst directly yields the dispersion of the sample: 20 ± 2%. The extent of hydrogen adsorption points to a dispersion of 14% (Table 1). This discrepancy may be attrib-

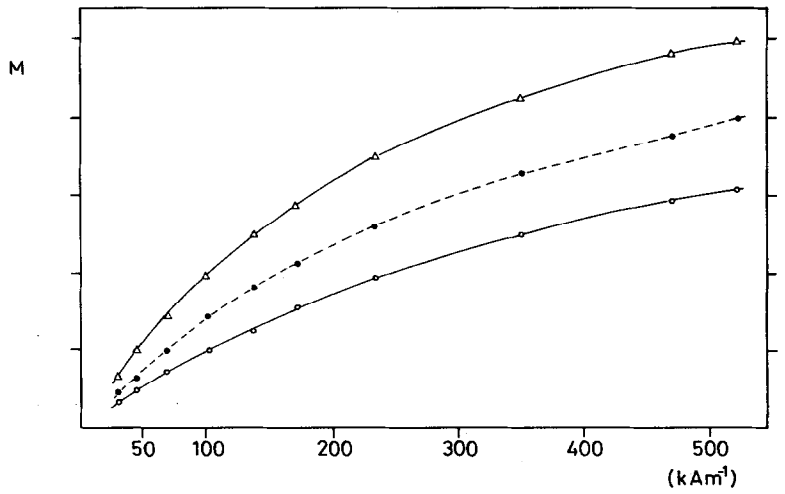

FIG. 6. Magnetization of the catalyst (in arbitrary units) at 298 K after exposure to N_2 (△), H_2 (●), CH_3OH (○).

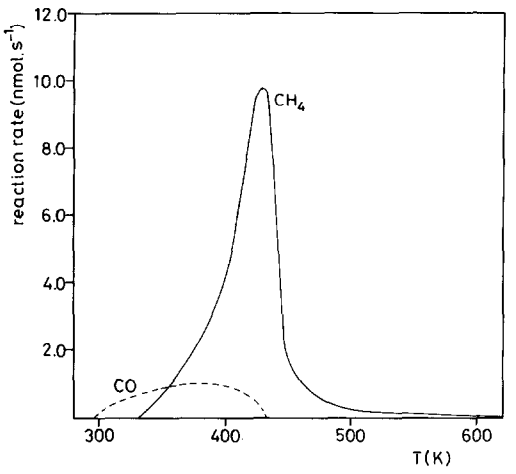

FIG. 7. TPH profile after exposure of the catalyst to methanol (6.5 kPa) at 520 K (flow, 1.0 ml/s 10% H_2/N_2; heating rate, 10 mK/s).

uted to (i) the possibly incorrect geometrical assumption (hemispherical particles) made in the evaluation of the dispersion using hydrogen adsorption and (ii) inadequacies of the extrapolation to saturation magnetization with nickel particles smaller than 5 nm (*30*). The deviation from the true saturation magnetization will be larger in the case of the smaller magnetic volumes of the hydrogen-covered nickel particles.

After saturation with hydrogen the catalyst was brought into a stationary state at a selected methanol pressure and temperature. After 3.6 ks of stationary-state operation, keeping the conversion to methane below 8% in order to achieve conditions comparable to those during the kinetic measurements, the methanol-containing flow was replaced by N_2 and the sample was quenched to room temperature. Then the saturation magnetization corresponding to the stationary-state coverage was measured ((○) in Fig. 6). Samples quenched from stationary state were analyzed using TPH or TPD. The results of TPH, TPD, and magnetic measurements were not significantly influenced by the details of the quenching procedure.

Figure 7 shows a TPH profile. A small CO peak is detected at a peak temperature of 387 ± 6 K, and a much larger CH_4 peak at 423 ± 3 K. The latter peak was shifted to lower temperatures (even room temperature) if performance under stationary-state conditions was followed by flushing the catalyst with nitrogen at 473 K for 3.6 ks before performing TPH. A typical TPD profile is presented in Fig. 8. Peak temperatures are 395 ± 4 K (CO), 473 ± 7 K (CO_2), 486 ± 2 K (CH_4), and 659 ± 6 K (CO). (Error boundaries here and throughout this paper denote standard deviations.) Other compounds, e.g., methanol and formaldehyde, were never detected. H_2 desorption was observed over practically the whole temperature range. The quantities desorbed were too small to allow accurate quantitative determination with the HWD, but the amount of H_2 detected was seen to increase on increasing the temperature.

The saturation magnetizations determined after TPH were equal to those obtained after adsorption of a monolayer of hydrogen. The saturation magnetization after TPD proved to be equal to the satura-

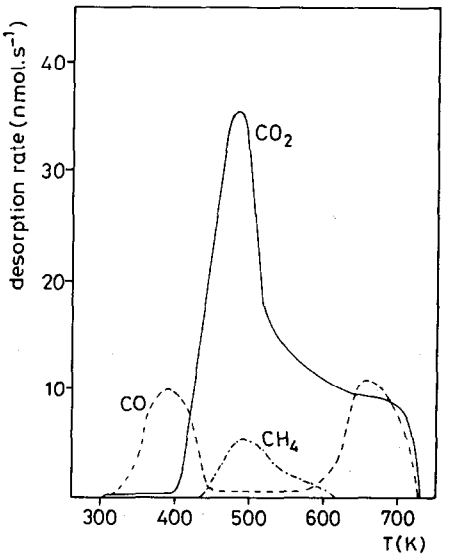

FIG. 8. TPD profile after exposure of the catalyst to methanol (6.5 kPa) at 520 K (flow, 0.7 ml/s N_2; heating rate, 10 mK/s).

TABLE 2

Fractional Surface Coverages Obtained with TPH, TPD, and Magnetic Measurements

Exposure to	Saturation magnetization × 100 / Saturation magnetization of clean cat.	Adsorbed carbonaceous species (monolayer equivalent)
N_2, 698 K	100 ± 2	
H_2, 723 K	80 ± 3	
CH_3OH, 473–583 K	60 ± 3	0.70 ± 0.12 (TPH) 0.77 ± 0.16 (TPD)

tion magnetization of the clean catalyst. Also, the original methanation activity was restored after both TPH and TPD. Performing a TPH run up to temperatures of 1073 K immediately after TPD showed that no carbonaceous species were left on the catalyst surface. Determination of surface coverages has been performed at a number of stationary states covering the range of experimental conditions. There was no apparent influence of the reaction conditions on the surface coverages during stationary state. The results are shown in Table 2.

DISCUSSION

Mechanism

As stated in the Introduction the advancement of the decomposition of methanol cannot be described by one simple stoichiometric reaction. We are dealing with a network of reactions in which a number of single reactions may proceed simultaneously or consecutively. Our first task therefore is identification of the possible reactions and analysis of the mechanisms by which they are produced.

A mechanism is defined as a sequence of elementary steps. The sequences that can be derived are determined by the set of elementary steps chosen. Since this choice depends on an interpretation of the experimental evidence, the set of elementary steps used may be incomplete or redundant. Redundancy in the set of elementary steps is easily traced. Omission of physically important steps can be detected only by experimentally testing kinetic rate equations derived from the reaction mechanism obtained. Whether such an omission is actually found depends on the quality of the kinetic data and the differences in the functional form of the rate equations.

In Table 3 the elementary steps that have been chosen to describe the methanol decomposition are listed. It should be noted that elementary steps involving either hydrogen-assisted CO dissociation or dissociation of oxygen or hydroxyl from adsorbed methoxy intermediates have not been included in the set. These elementary steps have been proposed from experiments conducted under transient conditions (*31*, *32*).

TABLE 3

Set of Elementary Steps Used to Describe Methanol Decomposition

s_1	$CH_3OH(g)$	$+ s$	$\rightleftharpoons CH_3OH(ad)$		
s_2	$CH_3OH(ad)$	$+ s$	$\rightleftharpoons CH_3O(ad)$	$+ H(ad)$	
s_3	$CH_3O(ad)$	$+ s$	$\rightleftharpoons CH_2(ad)$	$+ H(ad)$	
s_4	$CH_2O(ad)$	$+ s$	$\rightleftharpoons CHO(ad)$	$+ H(ad)$	
s_5	$CHO(ad)$	$+ s$	$\rightleftharpoons CO(ad)$	$+ H(ad)$	
s_6	$CO(ad)$		$\rightleftharpoons CO(g)$	$+ s$	
s_7	$2H(ad)$		$\rightleftharpoons H_2(g)$	$+ 2s$	
s_8	$CO(ad)$	$+ s$	$\rightleftharpoons C(ad)$	$+ O(ad)$	
s_9	$C(ad)$	$+ H(ad)$	$\rightleftharpoons CH(ad)$	$+ s$	
s_{10}	$CH(ad)$	$+ H(ad)$	$\rightleftharpoons CH_2(ad)$	$+ s$	
s_{11}	$CH_2(ad)$	$+ H(ad)$	$\rightleftharpoons CH_3(ad)$	$+ s$	
s_{12}	$CH_3(ad)$	$+ H(ad)$	$\rightleftharpoons CH_4(ad)$	$+ s$	
s_{13}	$CH_4(ad)$		$\rightleftharpoons CH_4(g)$	$+ s$	
s_{14}	$O(ad)$	$+ H(ad)$	$\rightleftharpoons OH(ad)$	$+ s$	
s_{15}	$OH(ad)$	$+ H(ad)$	$\rightleftharpoons H_2O(ad)$	$+ s$	
s_{16}	$H_2O(ad)$		$\rightleftharpoons H_2O(g)$	$+ s$	
s_{17}	$O(ad)$	$+ CO(ad)$	$\rightleftharpoons CO_2(ad)$	$+ s$	
s_{18}	$CO_2(ad)$		$\rightleftharpoons CO_2(g)$	$+ s$	

There is no evidence for the occurrence of these steps under stationary-state conditions (*14–16*). Our own experimental results concerning the above steps will be discussed later.

A method to derive all physically acceptable mechanisms from a chosen set of elementary steps has recently been published by Happel and Sellers (*18*). A brief outline of their procedure will be given here, but the reader is referred to the original literature for the details of this procedure. Mathematically the elementary steps can be considered a basis for the construction of all possible mechanisms. This implies that all possible mechanisms can be obtained by linear combination of the elementary steps. However, we are not interested in all mechanisms, but only in steady-state mechanisms, i.e., mechanisms which lead to reactions containing only terminal species (the reactants and products appearing in an overall reaction) and no intermediates. To obtain all steady-state mechanisms the elementary steps are rewritten in such a way that the basis for the reaction system can be divided into three disjoint bases. These three bases describe respectively (i) the non-steady-state mechanisms, involving both intermediates and terminal species; (ii) the steady-state mechanisms, involving only terminal species; and (iii) the cycles, which do not result in a net reaction, but can be necessary for a chemically correct description of the reaction system. To obtain the three bases the elementary steps are arranged in a step-by-species matrix. The matrix is put into a diagonal form by means of elementary row operations and column permutations.

In Fig. 9 the diagonalized step-by-species matrix for methanol decomposition is represented. The first 15 elementary steps in the matrix correspond to non-steady-state mechanisms, the last three to steady-state mechanisms. It is seen that due to the choice of elementary steps there are no cycles in the system. The three mechanisms denoted m_{16}, m_{17}, and m_{18} therefore form a basis for all steady-state mechanisms. The most general steady-state mechanism can thus be written as a linear combination of

		CH_3OH (ad)	CH_3O (ad)	CH_2O (ad)	CHO (ad)	C (ad)	CH (ad)	CH_2 (ad)	CH_3 (ad)	CH_4 (ad)	OH (ad)	H_2O (ad)	O (ad)	CO (ad)	CO_2 (ad)	H (ad)	S	CH_3OH (g)	CH_4 (g)	CO (g)	CO_2 (g)	H_2 (g)	H_2O (g)
m_1	S_2	-1	1	0	0	0	0	0	0	0	0	0	0	0	0	1	-1	0	0	0	0	0	0
m_2	S_3	0	-1	1	0	0	0	0	0	0	0	0	0	0	0	1	-1	0	0	0	0	0	0
m_3	S_4	0	0	-1	1	0	0	0	0	0	0	0	0	0	0	1	-1	0	0	0	0	0	0
m_4	S_5	0	0	0	-1	0	0	0	0	0	0	0	0	1	0	1	-1	0	0	0	0	0	0
m_5	S_9	0	0	0	0	-1	1	0	0	0	0	0	0	0	0	-1	1	0	0	0	0	0	0
m_6	S_{10}	0	0	0	0	0	-1	1	0	0	0	0	0	0	0	-1	1	0	0	0	0	0	0
m_7	S_{11}	0	0	0	0	0	0	-1	1	0	0	0	0	0	0	-1	1	0	0	0	0	0	0
m_8	S_{12}	0	0	0	0	0	0	0	-1	1	0	0	0	0	0	-1	1	0	0	0	0	0	0
m_9	S_{13}	0	0	0	0	0	0	0	0	-1	0	0	0	0	0	0	1	0	1	0	0	0	0
m_{10}	S_{15}	0	0	0	0	0	0	0	0	0	-1	1	0	0	0	-1	1	0	0	0	0	0	0
m_{11}	S_{16}	0	0	0	0	0	0	0	0	0	0	-1	0	0	0	0	1	0	0	0	0	0	1
m_{12}	S_{17}	0	0	0	0	0	0	0	0	0	0	0	-1	-1	1	0	1	0	0	0	0	0	0
m_{13}	S_6	0	0	0	0	0	0	0	0	0	0	0	0	-1	0	0	1	0	0	1	0	0	0
m_{14}	S_{18}	0	0	0	0	0	0	0	0	0	0	0	0	0	-1	0	1	0	0	0	1	0	0
m_{15}	S_7	0	0	0	0	0	0	0	0	0	0	0	0	0	0	-2	2	0	0	0	0	1	0
m_{16}	$S_1+S_2+S_3+S_4+S_5+S_6+2\cdot S_7$	0	0	0	0	0	0	0	0	0	0	0	0	0	0	0	0	-1	0	1	0	2	0
m_{17}	$S_8+S_9+S_{10}+S_{11}+S_{12}+S_{13}+S_{17}+S_{18}-2\cdot S_7-2\cdot S_6$	0	0	0	0	0	0	0	0	0	0	0	0	0	0	0	0	0	1	-2	1	-2	0
m_{18}	$S_6+S_{14}+S_{15}+S_{16}-S_{18}-S_{17}-S_7$	0	0	0	0	0	0	0	0	0	0	0	0	0	0	0	0	0	0	1	-1	-1	1

FIG. 9. Diagonalized step-by-species matrix for methanol decomposition.

m_{16}, m_{17}, and m_{18} according to

$$m = \rho m_{16} + \sigma m_{17} + \tau m_{18}. \quad (3)$$

Substituting the explicit expressions for the mechanisms m_{16}–m_{18} taken from Fig. 9 and rewriting yields

$$\begin{aligned} m = {} & \rho s_1 + \rho s_2 + \rho s_3 + \rho s_4 + \rho s_5 \\ & + (\tau - 2\sigma + \rho)s_6 + (2\rho - 2\sigma \\ & - \tau)s_7 + \sigma s_8 + \sigma s_9 + \sigma s_{10} \\ & + \sigma s_{11} + \sigma s_{12} + \sigma s_{13} + \tau s_{14} \\ & + \tau s_{15} + \tau s_{16} + (\sigma - \tau)s_{17} \\ & + (\sigma - \tau)s_{18} \end{aligned} \quad (4a)$$

$$\begin{aligned} m = {} & \rho(s_1 + s_2 + s_3 + s_4 + s_5) \\ & + (\tau - 2\sigma + \rho)s_6 + (2\rho - 2\sigma \\ & - \tau)s_7 + \sigma(s_8 + s_9 + s_{10} + s_{11} \\ & + s_{12} + s_{13}) + \tau(s_{14} + s_{15} + s_{16}) \\ & + (\sigma - \tau)(s_{17} + s_{18}). \end{aligned} \quad (4b)$$

The ρ, σ, and τ in these formulas describe the number of occurrences of each elementary step for a single occurrence of the overall reaction.

In accordance with the formulation of the general steady-state mechanism, the general overall reaction [$R = \Sigma\, \nu_i A_i$, in which ν_i is the stoichiometric coefficient (positive for products, negative for reactants) and A_i stands for the chemical participating in the reaction] can be written as

$$\begin{aligned} R = {} & \rho(-CH_3OH + CO + 2H_2) \\ & + \sigma(-2CO - 2H_2 + CH_4 \\ & + CO_2) + \tau(-CO_2 - H_2 + CO \\ & + H_2O) \end{aligned} \quad (5a)$$

$$\begin{aligned} R = {} & (\rho - 2\sigma + \tau)CO + (2\rho - 2\sigma - \tau)H_2 \\ & - \rho CH_3OH + \sigma CH_4 \\ & + \tau H_2O + (\sigma - \tau)CO_2. \end{aligned} \quad (5b)$$

To illustrate the sufficiency of our basis set of elementary steps we will distinguish the following cases.

(i) At low residence times we know the overall reaction to be

$$CH_3OH \rightleftharpoons CO + 2H_2. \quad (1)$$

Equation (5b) shows that σ and τ are zero at low residence times. Substituting this result in Eq. (4b) leads to the mechanism producing reaction (1):

$$\begin{aligned} m = {} & \rho(s_1 + s_2 + s_3 + s_4 \\ & + s_5 + s_6 + 2s_7). \end{aligned} \quad (6)$$

(ii) The overall reaction corresponding to the equilibrium at a temperature of 500 K (see Eq. (2)) can be obtained by substituting $3\rho = 4\sigma = 6\tau$ in Eq. (5b). Substitution of these values in the general overall mechanism (Eq. (4)) yields the mechanism corresponding to this reaction. Changes in the equilibrium composition at more elevated temperatures can be explained by an increase of ρ and a decrease of τ relative to σ.

(iii) Under differential conditions no CO_2 formation was observed (see Fig. 2). By inspection of Eq. (5b) it can be readily seen that σ must equal τ under these conditions. Equation (4b) is thus reduced to

$$\begin{aligned} m = {} & \rho(s_1 + s_2 + s_3 + s_4 + s_5) \\ & + (\rho - \sigma)s_6 + (2\rho - 3\sigma)s_7 \\ & + \sigma(s_8 + s_9 + s_{10} + s_{11} + s_{12} \\ & + s_{13} + s_{14} + s_{15} + s_{16}). \end{aligned} \quad (7)$$

The elementary steps s_1 to s_5 proceed consecutively and at the same relative rate, which is characterized by ρ. Therefore, we may consider the reaction

$$CH_3OH(g) + 5s \rightleftharpoons CO(ad) + 4H_{ad} \quad (8)$$

to proceed at the relative rate ρ. Accordingly, we can see that the sequences of elementary steps leading to the reactions

$$CO(ad) + 4H(ad) \rightleftharpoons CH_4(g) + O(ad) + 4s \quad (9)$$

$$O(ad) + 2H(ad) \rightleftharpoons H_2O(g) + 3s \quad (10)$$

proceed at the relative rate σ, hydrogen desorption at the relative rate $(2\rho - 3\sigma)$, and carbon monoxide desorption at the relative rate $(\rho - \sigma)$.

From Fig. 2 it is apparent that the quantities of CO and H_2 in the product mixture greatly exceed the amount of CH_4. This im-

plies that ρ is much larger than σ; i.e., the number of occurrences of the reaction to CO and H_2 is much larger than the number of occurrences of the CO hydrogenation reaction. The reactions

$$CH_3OH \rightleftharpoons CO + 2H_2 \quad (1)$$

$$CO + 3H_2 \rightleftharpoons CH_4 + H_2O \quad (11)$$

can thus be considered to proceed independently; i.e., the rates are not interrelated. As σ is much smaller than ρ, the rate of CH_4 formation is determined by the rate of CO hydrogenation. This contention is confirmed by the good agreement between the rates of methane formation via methanol decomposition on the one hand and methanation rates from CO/H_2 mixtures on the other (see Fig. 5).

According to the mechanism (Eq. (7)), oxygen is removed from the catalyst surface as water and elementary steps leading to carbon dioxide are not necessary to describe the reaction system under differential conditions. The rates of formation of methane and water are equal. Preferred removal of oxygen via water formation is in line with earlier studies (*33, 34*).

Kinetics

The pressure and temperature dependences of the observed rate equations can be concisely summarized using a power rate law. All 159 data sets could be fitted to the empirical rate equation

$$TOF = (6.4 \pm 0.6)10^8 e^{-(119\pm4)/RT} p^{(0.44\pm0.01)}. \quad (12)$$

In this equation the activation energy is given in kJ/mol, $R = 8.314 \times 10^{-3}$ kJ/(mol K), T is the absolute temperature (K), p is the initial methanol pressure (kPa), and TOF stands for the turnover frequency (s^{-1}).

The parameters were obtained by simultaneously fitting all data using a nonlinear least-squares method. A Gauss–Newton algorithm was employed to find the solution (*35, 36*). The observed turnover frequencies as well as the apparent activation energies agree well with previously reported values for methanation from CO/H_2 mixtures (*37–39*). However, no mechanistic information can be obtained by fitting data to a power rate law.

A rate equation is most directly derived from a proposed mechanism using only the steady-state approximation. Unfortunately, the resulting equations become completely unmanageable and it turns out to be necessary to make the simplifying assumption that one step in the sequence is rate-determining. All steps preceding the rate-determining step are considered to be in equilibrium. Adsorption equilibria are assumed to be of the Langmuir type and the rate-determining step is supposed to be a reaction between adsorbed species. These assumptions are generally referred to as the Langmuir–Hinshelwood–Hougen–Watson (LHHW) approach. Assuming the rates of backward reactions to be negligible, it leads to rate equations of the form

$$TOF = \prod_i k_i p_i^{\alpha_i} \Big/ \left(1 + \sum_j k_j p_j^{\beta_j}\right)^{\gamma}. \quad (13)$$

The $p_{i,j}$ in this equation are partial pressures; the $k_{i,j}$ are products of equilibrium constants and rate constants; and α_i, β_j, and γ are real numbers, often integers or zero. Unlike the parameters of a power rate law, the parameters of a LHHW-type rate equation can, in principle, be related to quantities having physical significance, such as enthalpies and entropies of adsorbed species. Moreover, a LHHW-type rate equation predicts the coverages of intermediates, which can be compared with independent determinations of concentrations of adsorbed species.

Due to the interdependence of the parameters, confidence intervals of individual parameters are rather large. Rationalization of the estimated parameters, eventually leading to the enthalpy and entropy of the activated complex, is therefore not possible without introducing serious uncertainties.

TABLE 4

Rate Equations for Different Positions of the Rate-Determining Step in the Mechanism ($Q_i = A_i e^{E/RT}$)

Rate-determining step	Rate equation
s_8,	(a) TOF = $Q_3 p/(1 + Q_2 p^{0.5} + Q_1 p)^2$
s_9, s_{14}	(b) TOF = $Q_3 p/(1 + Q_2 p^{0.5} + Q_1 p)^2$
s_9, s_{15}	(c) TOF = $Q_5 p^{1.25}/(1 + Q_4 p^{0.25} + Q_3 p^{0.5} + Q_2 p^{0.75} + Q_1 p)^2$
s_{10}, s_{14}	(d) TOF = $Q_5 p^{1.25}/(1 + Q_4 p^{0.25} + Q_3 p^{0.5} + Q_2 p^{0.75} + Q_1 p)^2$
s_{10}, s_{15}	(e) TOF = $Q_3 p^{1.5}/(1 + Q_2 p^{0.5} + Q_1 p)^2$

The problem now is to discriminate between the rival models obtained by putting the rate-determining step at different positions in the sequence of elementary steps. The different rate equations thus obtained have been collected in Table 4. In the Appendix an example of the derivation of a rate equation is given. The suggestion that CO dissociation is rate-determining (*40, 41*) could not be confirmed. This can be appreciated by inspection of the resulting rate equation (Eq. (a) in Table 4). To a good approximation we can assume the fraction of free sites to be very small, allowing us to neglect the constant 1 in the denominator. The equation now reduces to

$$\text{TOF} = A_3 e^{E/RT}/(A_2 e^{E/RT} + A_1 e^{E/RT} p^{0.5})^2. \quad (14)$$

As can be seen from this equation the maximum order in methanol pressure is zero when the fraction of free sites is small. Since our experimental value equals 0.44, CO dissociation is very unlikely to be rate-determining. For the same reason C(ad) hydrogenation is unlikely to be rate-determining when O(ad) hydrogenation is co-rate-determining (see Table 4). Unfortunately, discrimination between the other CH_x(ad) hydrogenation steps was not possible on the basis of the present data. Following earlier investigations (*42–43*) we have worked out (e) from Table 4. Parameter estimations for this model have been collected in Table 5. A plot of residuals is shown in Fig. 10. The uniform distribution of the residuals confirms the adequacy of the rate equation. It should be noted that a change of rate-determining step was not invoked to explain changes in apparent activation energies over our range of temperatures and pressures. The observed changes can be fully explained by changes in the adsorption equilibria.

We believe that the main strength of LHHW rate equations relative to empirical rate equations is to be found in the capability of the former to predict coverages of intermediates. As the evaluation of surface coverages at a given temperature and pressure always involves combinations of exponentials and preexponentials a reasonable indication of the surface coverages can be obtained. The surface coverages as derived from fitting the kinetic data to Eq. (e) of Table 4 are shown in Fig. 11.

TABLE 5

Parameters Estimated from Fitting the Data to Eq. (e) of Table 4

Parameter	Value	Dimension
k_1	1.2×10^{-8}	kPa^{-1} s^{-1}
E_1	-6.8×10^{1}	kJ mol^{-1}
k_2	1.8×10^{-1}	kPa$^{-1/2}$
E_2	1.5×10^{1}	kJ mol^{-1}
k_3	3.1×10^{-16}	kPa^{-1}
E_3	1.4×10^{2}	kJ mol^{-1}

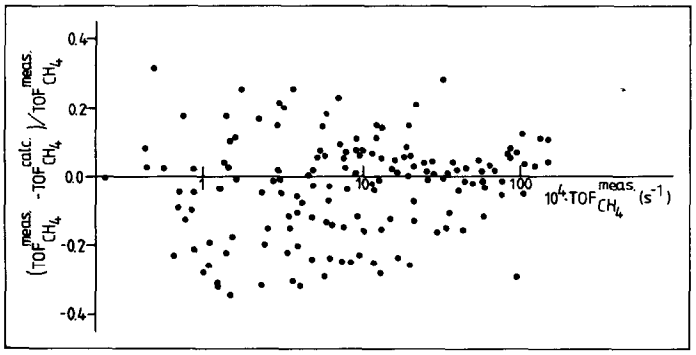

FIG. 10. Distribution of residuals. Relative deviations of the calculated values are plotted as a function of measured rates.

Surface Coverages

We now turn to the surface coverages obtained with TPH, TPD, and magnetic measurements. The TPD results show that the main carbon-containing species on the surface is CO. When TPH is performed part of this CO desorbs, while a much larger part dissociates and is hydrogenated to CH_4 (and H_2O). No separate CH_4 peak at low temperatures due to the hydrogenation of the more active C(ad) (*44, 45*) could be detected with samples quenched from the stationary state. The observation that methane is already formed at room temperature if part of the CO is allowed to desorb and/or decompose is consistent with the work of Rabo *et al.* (*46*). They showed that the reactivity of C(ad) toward hydrogenation greatly decreases with increasing CO coverage. Apparently due to the large CO coverages during the stationary state C(ad) hydrogenation does not occur before the temperature is raised to about 350 K and part of the CO has desorbed, thus making the separation of C(ad) and CO contributions to the observed TPH profile impossible. It should be mentioned that peak temperatures reported in this work are somewhat lower than those reported previously (*41*), because of the low heating rate used.

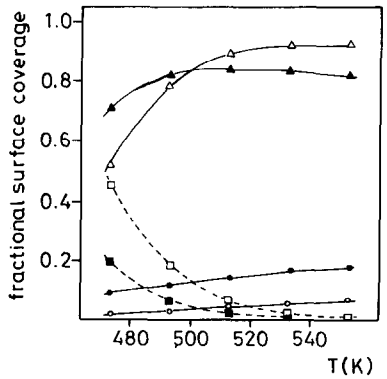

FIG. 11. Fractional surface coverages (○, free sites; △, H(ad) + C(ad) + O(ad); □, OH(ad) + CO(ad) + CH(ad)) as a function of temperature calculated from the estimated parameters (Table 5). Solid symbols refer to a pressure of 0.8 kPa, open symbols to 8 kPa.

During TPH or TPD no desorption of methanol or formaldehyde was observed, which indicates that adsorbed quantities of these species are very low, if existent at all. The total amount of carbon detected during TPD, viz. 0.7 monolayer, agrees well with the total amount detected during TPH. This is somewhat surprising. One would expect the amount of carbon-containing species detected during TPD to be lower due to the Boudouard reaction, leaving one carbon atom on the surface for every desorbed CO_2 molecule. However, by magnetic measure-

ments, by inspection of the methane turnover frequencies, and by performance of TPH at elevated temperatures after TPD, the catalyst surface appeared to be free from carbonaceous species after TPD. Obviously the carbon deposited in the Boudouard reaction is oxygenated during the TPD experiment. In our opinion the most probable source of oxygen atoms is water desorbing from the silica support. The reactivity of adsorbed carbon toward water has been well established (*47*). Alternatively, carbon dioxide can be formed via reaction of adsorbed carbon monoxide with water. It should be noted that in contrast to the work of Biloen *et al.* (*42*) and McCarty and Wise (*48*) no appreciable buildup of less active carbonaceous species was observed, even in cases where the stationary state was maintained for several hours.

A most interesting result is that the decrease in saturation magnetization of samples quenched from the stationary state is about twice the decrease caused by adsorption of a monolayer of hydrogen. From the TPD experiments it has been deduced that almost all carbon is present as CO. Since adsorbed CO is partly present in a multibonded form, the amount of CO causes a decrease in magnetization corresponding to the decoupling of about one monolayer of Ni atoms. The additional decrease in magnetization can be due to the presence of hydrogen, carbon dissolved in the bulk of the catalyst, or oxygen. We do not believe the presence of oxygen to be of importance, as nickel oxide is stable under TPD conditions. Also, Goodman *et al.* (*49*), using AES, could not detect oxygen on a Ni(100) surface after stationary-state exposure to CO/H_2. According to Cant and Bell (*50*) the inventory of oxygen on Ru is undetectable. Since almost all of the carbon is present in the form of CO, the amount of dissolved carbon will be very low and cannot account for the decoupling of an additional monolayer equivalent of Ni atoms, despite the high decoupling effect (up to seven nickel atoms per carbon atom) reported for dissolved carbon. Therefore, we believe that the additional magnetization decrease is mainly due to adsorbed hydrogen.

Carbon monoxide and hydrogen have been reported to coadsorb attractively, both in approximately monolayer amounts on supported transition metal catalysts at temperatures near 400 K. Horgan and King (*51*) observed mutual enhancement of CO and H_2 on Ni up to temperatures of 648 K. Very recently Winslow and Bell (*52*) have shown that monolayer amounts of both CO(ad) and H(ad) are present during CO hydrogenation over Ru. The observation that the adsorbed hydrogen is magnetically active, i.e., is magnetically decoupling one monolayer equivalent of nickel atoms, makes it unlikely that hydrogen is present in CH_xO species. The observation that two monolayer equivalents of nickel atoms are decoupled suggests that hydrogen is displaced by carbon monoxide to subsurface positions, e.g., the second layer positions in the more open planes. It has been suggested previously (*53*) that hydrogen is displaced to subsurface positions if recombination of adsorbed hydrogen is hampered by the presence of large amounts of preferentially adsorbed ad species.

Because from magnetic measurements and from TPD and TPH the existence of CH_xO intermediates proves to be unlikely, we have not included elementary steps involving CH_xO(ad) in the analysis of the reaction system.

Comparison of the surface coverages calculated from the estimated parameters with those obtained from TPH, TPD, and magnetic measurements shows large differences. However, we stress that from the measurements total surface coverages are obtained, whereas the surface coverages calculated from the rate equation are related to the coverage of the active sites only. From dilution of nickel with inactive copper it emerged that specific ensembles are required for the dissociation of carbon monoxide (*44, 54*). Decomposition of methanol into CO and H_2 is assumed to be much

faster, because the C–O bond is not broken in this case and thus the special sites are not required here. This is a plausible physical explanation for ρ being much larger than σ in Eq. (7).

The question arises why CH_x hydrogenation is so often found to be the rate-limiting step, notwithstanding the presence of the equivalent of an almost complete monolayer of adsorbed hydrogen. From our TPH on a partially covered surface as well as from experiments where CO is abruptly removed from the feed (*32, 55*), it follows that small changes in total CO coverage drastically influence the CH_x hydrogenation rate. We speculate that a major part of the total hydrogen coverage is displaced by CO to positions where it is relatively immobile. Only H(ad) on the surface readily reacts with C(ad) to form methane. The limited quantities of hydrogen adsorbed on the surface may well explain the observation that CH_x hydrogenation is rate-determining under our conditions. Such a description of the reaction system could also explain observed changes in the rate-determining step (CO dissociation versus CH_x hydrogenation) and the sensitive influence of the CO/H_2 ratio (*40, 56*), but much work remains to be done to fully elucidate the reaction system.

CONCLUSIONS

(*i*) The formation of methane from methanol under differential conditions can be described in terms of two consecutive reactions. Methanol first decomposes into CO and H_2, followed by methanation of carbon monoxide. The former reaction is much faster than the latter.

(*ii*) Kinetic data can be fitted to a LHHW rate equation involving the hydrogenation of a CH intermediate as the rate-determining step. Hydrogen-assisted CO dissociation is not needed to describe the data.

(*iii*) Large discrepancies have been observed in total surface coverages determined with TPH, TPD, and magnetic measurements on the one hand and the surface coverages predicted by the LHHW rate equation on the other. This has been interpreted as an indication that only a minor fraction of the surface sites is actually involved in the methanation reaction.

APPENDIX

We must consider the gas phase reactions

$$CH_3OH \rightleftharpoons CO + 2H_2 \qquad (A1)$$

$$CO + 3H_2 \rightleftharpoons CH_4 + H_2O. \qquad (A2)$$

Reaction (A1) is considered to proceed much faster than reaction (A2). Also, the equilibrium of (A1) is completely to the CO + $2H_2$ side; thus every CH_3OH molecule adsorbing on the surface results in the adsorption of CO(ad) and 4H(ad). The adsorbed amounts of CO_{ad} and H_{ad} are in equilibrium with a virtual CO pressure, respectively, H_2 pressure. These virtual pressures equal the equilibrium pressures of CO and H_2 for reaction (A1). That is, CO(ad) and H(ad) are in equilibrium with a virtual CO and H_2 pressure, which equals the initial (inlet) methanol partial pressure (*57*),

$$P_{CO} = p^{init}_{methanol} \qquad (A3)$$

$$p_{H_2} = 2p^{init}_{methanol}. \qquad (A4)$$

This concept of virtual pressures has been confirmed in experiments in which a $CO/H_2 = \frac{1}{2}$ mixture was used instead of methanol: the observed rates of reaction are the same when the CO partial pressure in the mixture equals the methanol pressure.

Since the rate of reaction (A2) is much lower than the rate of reaction (A1), one of the elementary steps leading to reaction (A2) must be rate-determining. In this derivation we will assume CH hydrogenation to be rate-determining. Because the rate of water formation must equal the rate of methane formation, OH hydrogenation has been chosen as the co-rate-determining step. All steps preceding the rate-determining step are considered to be in equilibrium;

all steps succeeding the rate-determining step are considered to be kinetically unimportant. When, as generally, the assumption is made that only a single type of reaction site exists (thus neglecting the possibility of active ensembles) the mechanism can be written as

$$CH_3OH(g) \rightleftharpoons CO(g) + 2H_2(g) \quad (A1)$$

$$CO(g) + s \rightleftharpoons CO(ad) \quad (A5a)$$

$$CO(ad) + s \rightleftharpoons C(ad) + O(ad) \quad (A6a)$$

$$H_2(g) + 2s \rightleftharpoons 2H(ad) \quad (A7a)$$

$$O(ad) + H(ad) \rightleftharpoons OH(ad) + s \quad (A8a)$$

$$OH(ad) + H(ad) \rightarrow H_2O(g) + 2s \quad (A9)$$

$$C(ad) + H(ad) \rightleftharpoons CH(ad) + s \quad (A10a)$$

$$CH(ad) + H(ad) \rightarrow CH_2(ad) + s \quad (A11a)$$

$$CH_2(ad) + 2H(ad) \rightleftharpoons CH_4(g) + 3s. \quad (A12a)$$

The rate can be expressed as

$$r = k_{11}\theta_{CH}\theta_H = k_9\theta_{OH}\theta_H \quad (A11b)$$

$$\theta_{CH}/\theta_{OH} = k_9/k_{11}. \quad (A11c)$$

The equilibrium constants can be written as

$$K_5 = \theta_{CO}/(p_{CO}\theta_s) \quad (A5b)$$

$$K_6 = (\theta_C\theta_O)/(\theta_{CO}\theta_s) \quad (A6b)$$

$$K_7 = \theta_H^2/(p_{H_2}\theta_s^2) \quad (A7b)$$

$$K_8 = (\theta_{OH}\theta_s)/(\theta_H\theta_O) \quad (A8b)$$

$$K_{10} = (\theta_{CH}\theta_s)/(\theta_H\theta_C). \quad (A10b)$$

θ's in the above formulas denote fractional coverages. They are related by

$$1 = \theta_s + \theta_{CO} + \theta_{CH} + \theta_{OH} + \theta_H + \theta_O + \theta_C. \quad (A12b)$$

Using the equations (A3), (A4), (A5b)–(A8b), (A10b), (A11c) all surface coverages can be expressed in terms of the fraction of free sites (θ_s) and the initial methanol pressure (denoted p in the following):

$$\theta_s = \theta_s \quad (A13a)$$

$$\theta_{CO} = \theta_s K_5 p_{CO} = \theta_s A p \quad (A13b)$$

$$\theta_{OH} = \theta_s(K_5K_6K_7K_8K_{10}k_{11}p_{CO}p_H/k_9)^{0.5} = \theta_s B p \quad (A13c)$$

$$\theta_{CH} = \theta_s(K_5K_6K_7K_8K_{10}k_9p_{CO}p_H/k_{11})^{0.5} = \theta_s C p \quad (A13d)$$

$$\theta_H = \theta_s(K_7p_H)^{0.5} = \theta_s D p^{0.5} \quad (A13e)$$

$$\theta_O = \theta_s(K_5K_6K_{10}k_{11}p_{CO}/K_8k_9)^{0.5} = \theta_s E p^{0.5} \quad (A13f)$$

$$\theta_C = \theta_s(K_5K_6K_8k_9p_{CO}/K_{10}k_{11})^{0.5} = \theta_s F p^{0.5}. \quad (A13g)$$

Substituting the above in Eq. (A12) leads to

$$1 = \theta_s(1 + \{A + B + C\}p + \{D + E + F\}p^{0.5}) \quad (A14a)$$

$$1 = \theta_s(1 + Q_1p + Q_2p^{0.5}). \quad (A14b)$$

The rate of methanation is

$$r = k_{11}\theta_{CH}\theta_H = k_{11}CDp^{1.5}\theta_s^2 = Q_3p^{1.5}\theta_s^2. \quad (A15)$$

Substituting (A14b) for θ_s leads to

$$r = Q_3p^{1.5}/(1 + Q_1p + Q_2p^{0.5})^2. \quad (A16)$$

In this equation every Q can be written as an Arrhenius-like product. The surface coverages can be derived directly from Eq. (A13):

$$\theta_{CO} + \theta_{CH} + \theta_{OH} = Q_1p/(1 + Q_1p + Q_2p^{0.5}) \quad (A17a)$$

$$\theta_H + \theta_C + \theta_O = Q_2p^{0.5}/(1 + Q_1p + Q_2p^{0.5}). \quad (A17b)$$

ACKNOWLEDGMENTS

The authors are indebted to Dr. A. J. H. M. Kock and Mr. W. Klop for helpful discussions. The computational assistance of Mr. A. van der Steen and Mr. C. A. Pietersen is gratefully acknowledged. The investigations were financially supported by the VEG-Gasinstituut n.v.

REFERENCES

1. Kojima, I., Sugihara, H., Miyazaki, E., and Yasumori, I., *J. Chem. Soc. Faraday Trans. 1* **77,** 1315 (1981).
2. Steinbach, F., and Schuette, J., *Surf. Sci.* **146,** 534 (1984).
3. Johnson, S., and Madix, R. J., *Surf. Sci.* **103,** 361 (1981).
4. Yates, J. T., Jr., Goodman, D. W., and Madey, T. E., *in* "Proceedings, 7th Int. Vac. Congr. and 3rd Int. Conf. on Solid Surf. Vienna, 1977," p. 113.
5. Demuth, J. E., and Ibach, H., *Chem. Phys. Lett.* **60,** 395 (1979).
6. Yasumori, I., Nakamura, T., and Miyazaki, E., *Bull. Chem. Soc. Japan.* **40,** 1372 (1967).
7. Steinbach, F., and Sprengler, H.-J., *Surf. Sci.* **104,** 318 (1981).
8. Al-Mawlawi, D., and Saleh, J. M., *J. Chem. Soc. Faraday Trans. 1* **77,** 2965 (1981).
9. Roberts, M. W., and Stewart, T. I., *in* "Proceedings, Conf. Inst. Petrol., London, 1970" (P. Hepple, Ed.), p. 16.
10. Chang, C. D., *Catal. Rev. Sci. Eng.* **25,** 1 (1983).
11. Inui, T., Suehiro, M., Yamamoto, S., Ohmura, K., and Takegami, Y., *J. Japan. Pet. Inst.* **25**(2), 121 (1982).
12. Kliman, M. L., *Energy* **8,** 859 (1983).
13. Othmer, D. F., *Oil Gas J.* **80**(44), 84 (1982).
14. Vannice, M. A., *in* "Catalysis, Science and Technology" (J. R. Anderson and M. Boudart, Eds.), Vol. 3, p. 139. Springer-Verlag, Berlin, 1982.
15. Biloen, P., and Sachtler, W. M. H., *Adv. Cat.* **30,** 165 (1981).
16. Kelley, R. D., and Goodman, D. W., *in* "The Chemical Physics of Solid Surfaces and Heterogeneous Catalysis" (D. A. King and P. B. Woodruff, Eds.), Vol. 4, p. 427. Elsevier, Amsterdam, 1982.
17. Boudart, M., "Kinetics of Chemical Processes." Prentice-Hall, Englewood Cliffs, NJ, 1968.
18. Happel, J., and Seller, P. H., *Adv. Catal.* **32,** 273 (1983).
19. van Dillen, A. J., Geus, J. W., Hermans, L. A. M., and van der Meyden, J., *in* "Proceedings, 6th International Congress on Catalysis, London, 1976" (G. C. Bond, P. B. Wells, and F. C. Tompkins, Eds.). Vol. 2, p. 677. The Chemical Society, London, 1976.
20. Kuijpers, E. G. M., Jansen, J. W., van Dillen, A. J., and Geus, J. W., *J. Catal.* **72,** 75 (1981).
21. Davydov, E. M., and Kharson, M. S., *Zh. Fiz. Khim.* **50,** 2984 (1976).
22. De Bokx, P. K., Kock, A. J. H. M., Boellaard, E., Klop, W., and Geus, J. W., *J. Catal.* **96,** 454 (1988).
23. Kock, A. J. H. M., de Bokx, P. K., Boellaard, E., Klop, W., and Geus, J. W., *J. Catal.* **96,** 468 (1988).
24. Koros, R. M., and Nowak, E. J., *Chem. Eng. Sci.* **22,** 470 (1967).
25. Madon, R. J., and Boudart, M., *Ind. Eng. Chem. Fundam.* **21,** 438 (1982).
26. White, W. B., Johnson, S. M., and Dantzig, G. B., *J. Chem. Phys.* **28,** 751 (1958).
27. NAG Program Library, Routine E04WAF.
28. Anderson, J. R., "Structure of Metallic Catalysts," p. 296. Academic Press, New York/London, 1975.
29. Selwood, P. W., "Chemisorption and Magnetization," p. 46. Academic Press, New York/London, 1975.
30. Richardson, J. T., and Desai, P, *J. Catal.* **42,** 294 (1976).
31. Van Ho, S. and Harriott, P., *J. Catal.* **64,** 272 (1980).
32. Mori, T., Masuda, H., Imai, H., Miyamoto, A., Baba, S., and Murakami, Y., *J. Phys. Chem.* **86,** 2753 (1982).
33. Klose, J., and Baerns, M., *J. Catal.* **85,** 105 (1984).
34. Otarod, M., Ozawa, S., Yin, F., Chew, M., Cheh, H. Y., and Happel, J., *J. Catal.* **84,** 156 (1983).
35. NAG Program Library, Routine E04HEF.
36. Froment, G. F., and Hosten, L. H., *in* "Catalysis, Science and Technology" (J. R. Anderson and M. Boudart, Eds.), Vol. 2, p. 97. Springer-Verlag, Berlin, 1981.
37. Bartholomew, C. H., Pannel, R. B., and Butler, J. L., *J. Catal.* **65,** 335 (1980).
38. Vannice, M. A., *J. Catal.* **44,** 152 (1976).
39. Sughrue, E. L., and Bartholomew, C. H., *Appl. Catal.* **2,** 239 (1982).
40. Dalla Betta, R. A., and Shelef, M., *J. Catal.* **49,** 383 (1977).
41. Zagli, A. E., Falconer, J. L., and Keenan, C. A., *J. Catal.* **56,** 453 (1979).
42. Biloen, P., Helle, J. N., van den Berg, F. G. A., and Sachtler, W. M. H., *J. Catal.* **81,** 450 (1983).
43. Van Meerten, R. Z. C., Vollenbroek, J. G., de Croon, M. H. J. M., van Nisselrooy, P. F. M. T., and Coenen, J. W. E., *Appl. Catal.* **3,** 29 (1982).
44. Araki, M., and Ponec, V., *J. Catal.* **44,** 439 (1976).
45. Biloen, P., Helle, J. N., and Sachtler, W. M. H., *J. Catal.* **58,** 95 (1979).
46. Rabo, J. A., Risch, A. P., and Poutsma, M. L., *J. Catal.* **53,** 295 (1978).
47. Kuijpers, E. G. M., Ph.D. thesis, State University of Utrecht, Utrecht, 1982.
48. McCarty, J. G., and Wise, H., *J. Catal.* **57,** 406 (1979).

49. Goodman, D. W., Kelley, R. D., Madey, T. E., and Yates, J. T., Jr., *J. Catal.* **63,** 226 (1980).

50. Cant, N. W., and Bell, A. T., *J. Catal.* **73,** 257 (1982).

51. Horgan, A. M., and King, D. A., *in* "Adsorption–Desorption Phenomena" (F. Ricca, Ed.), p. 329. Academic Press, New York/London, 1972.

52. Winslow, P., and Bell, A. T., *J. Catal.* **91,** 142 (1985).

53. Baranowski, B., *in* "Festkörperchemie" (V. Boldyrev and K. Meyer, Eds.), P. 364. VEP, Leipzig, 1973.

54. Dalmon, J. A., and Martin, G. A., *in* "Proceedings, 7th International Congress on Catalysis, Tokyo, 1980" (T. Seiyama and K. Tanabe, Eds.), p. 402, Amsterdam, 1981.

55. Underwood, R. P., and Bennett, C. O., *J. Catal.* **86,** 245 (1984).

56. Polizzotti, R. S., and Schwarz, J. A., *J. Catal.* **77,** 1 (1982).

57. Kenball, C., *Discuss. Faraday Soc.* **41,** 190 (1966).